DOI: 10.1021/ma902663n

Macromolecules
ARTICLE

Synthesis of Hollow Polymer Nanocapsules Exploiting Gold Nanoparticles as Sacrificial Templates

Cyrille Boyer,[†] Michael R. Whittaker,[†] Cecile Nouvel,[†,‡] and Thomas P. Davis*[,†]

[†]*Centre for Advanced Macromolecular Design (CAMD), School of Chemical Sciences and Engineering, The University of New South Wales, Sydney, NSW 2052, Australia, and* [‡]*Laboratoire de Chimie Physique Macromoléculaire, UMR 7568 CNRS-Nancy University, ENSIC, BP 20451, 54001 Nancy cedex, France*

Received December 3, 2009; Revised Manuscript Received January 6, 2010

ABSTRACT: This paper describes a new approach for the synthesis of hollow functional polymer nanocapsules, which exploits gold nanoparticles as sacrificial templates. Two different functional diblock polymers have been coassembled on the gold nanoparticles prior to gold removal. The block polymers (made by RAFT polymerization) consisted of a biocompatible polymer segment, either (poly(oligoethylene glycol) acrylate, P(OEG-A), or poly(hydroxylpropylacrylamide), P(HPMA) and a cross-linkable segment comprised of an alternating copolymer of styrene (Sty) and maleic anhydride (MA), (Sty-*alt*-MA). The block copolymers were assembled onto the GNP surfaces using a grafting "onto" methodology exploiting the high affinity of the RAFT end-groups for the gold surface. The anhydride group was utilized to cross-link the polymer layer. Finally, the gold cores were removed using aqua regia without affecting the integrity of the polymers chains or the nanocapsules. All reaction and assembly steps were characterized by employing a range of techniques, such as TEM, XPS, ATR−FTIR, DLS, and UV−visible spectroscopy.

Introduction

Nanoscale hollow polymer capsules offer a unique and versatile platform for applications in biotechnology;[1,2] including drug/gene controlled release and delivery,[3] protection/support of biologically active species in vivo[4] and for bioimaging applications.[5] Hollow polymer capsules can be synthesized using a diverse range of methods such as emulsion polymerization,[6] phase separation,[7] cross-linking of micelles,[8] or a through directed self-assembly process.[9−11] One particularly versatile method involves the coating of a sacrificial inorganic/organic template with polymer followed by stabilization via a cross-linking reaction.[12] The template is typically selected to be a readily removable inorganic nanoparticle, e.g., silica or gold. Caruso et al.[13] also described the use of organic polymer (e.g., polystyrene latexes) particles. Templates are selected so that their sizes (diameter) can be controlled easily, thus leading to hollow capsules with predetermined sizes. To ensure that the nanocapsules retain integrity on the removal of the template, a cross-linking strategy is often employed and this can be achieved using a number of alternative approaches;[14] for example, click reactions,[14−16] carbodiimide reactions (amine−acid reactions),[8,17−20] activated ester−amine reactions,[21,22] photoinduced reactions,[23] nucleophilic substitution (between 1,2-bis(2-iodoethoxy)ethane and amine) reactions[24] and disulfide based reactions[25,26]

In previous work, the layer-by-layer assembly approach has been adopted to assemble polymers on sacrificial templates.[27,28] Recent work has shown that well-defined polymers synthesized via RAFT[29] polymerization can be used to assemble around GNPs via binding to the gold surface[30] (exploiting the affinity of RAFT end-groups for gold surfaces[31−33]), as demonstrated for the first time by McCormick, Lowe, and Sumerlin et al.[34] In addition, RAFT end-group functionality can be transformed easily to thiol[35−37] or pyridyl disulfide end groups.[38−40] The RAFT−polymer approach has been exploited to synthesize a range of responsive and functional organic nanoparticles[41−44] or hybrid polymer/inorganic nanoparticles.[30,45−54] RAFT polymerization can also be used to impart additional functionality to the polymer so that cross-linking can be induced following patterning around the template.

Sodium cyanide etching is widely used to remove sacrificial gold cores.[22] Removal of the core can also be achieved by the use of other cyanide salts without damaging the polymer shell.[55] Cyanide compounds are however extremely toxic and there is an impetus to explore alternative etching approaches. One possible alternative to the use of cyanide compounds is aqua regia; a mixture of nitric and hydrochloric acids in a ratio of approximately 1:3. Aqua regia can be made easily as the precursor reactants are readily available. In addition, aqua regia has safety and environmental advantages over cyanide reactants. Gold solubilization is achieved by the production of Au^{3+} ions formed by the interaction of gold with nitric acid reacting with chloride ions forming chloroaurate ions. The acids undergo reaction and chlorine gas is produced which also reacts with the Au(s), producing the chloroaurate ion.

RAFT polymerization has been used previously to synthesize well-defined PEG acrylate[56,57] and HPMA polymers.[38,58] In addition, RAFT has been used for the living radical polymerization of alternating styrene-maleic anhydride copolymers.[59] Wooley et al.[60] describe the synthesis of cross-linked nanoparticles utilizing the reaction between maleic anhydride and amines. In the work described in this current paper, we use RAFT to make block copolymers containing biocompatible polymers (as demonstrated in a recent paper on the cytotoxicity of RAFT polymers[61]) and also cross-linking functionality to assemble round the gold nanoparticles (Scheme 1). The polymers were then cross-linked using a small diamine molecule. Removal of the gold cores with aqua regia resulted in the formation of stable, biocompatible, low cytotoxic and antifouling hollow polymer nanocapsules.

*Corresponding author. E-mail: t.davis@unsw.edu.au.

 Published on Web 01/25/2010

Scheme 1. Synthesis of Nano-Capsules Using Gold Nanoparticles as Sacrificial Templates: (1) Nanoparticle Assembly; (2) Cross-Linking; (3) GNP Core Removal

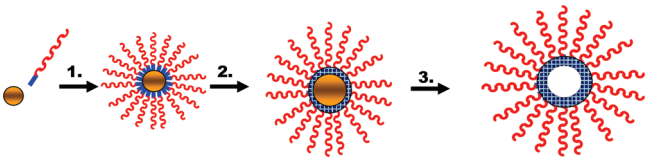

Experimental Section

1. Materials. Oligoethylene glycol acrylate (OEG-A) (Aldrich, number-average molecular weight M_n = 450 g/mol, PDI = 1.02) and styrene (Aldrich) were purified via a basic alumina column to remove the inhibitor prior to use. Maleic anhydride (Alrich) and hydroxylpropyl methacrylamide (Polymer Sciences, 99%) were used as received. 2,2′-Azobis-(isobutyronitrile) (AIBN) was purchased from Wako Chemicals and was crystallized twice from methanol prior to use. 1,2-Ethyldiamine (Aldrich, 99%), 1-ethyl-3-(3-(dimethylamino)-propyl) carbodiimide hydrochloride (EDC·HCl, Aldrich, 98%), hydrogenotetrachloroaurate(III) hydrate ($HAuCl_4$, 99.9%, Aldrich), and trisodium citrate dehydrate (99%, Aldrich) were used as received. Deionized water used for these experiments were purified by MILIQ system with a resistivity of 17.9 mΩ/cm.

2. Analytical Techniques. *2.1. Size Exclusion Chromatography (SEC).* SEC analyses of the polymers were performed in *N*,*N*-dimethylacetamide [DMAc; 0.03% w/v LiBr, 0.05% 2,6-dibutyl-4-methylphenol (BHT)] at 50 °C (flow rate = 1 mL/min) using a Shimadzu modular system comprised of an SIL-10AD autoinjector, a PL 5.0 mm bead-size guard column (50 × 7.8 mm) followed by four linear PL (Styragel) columns (10^5, 10^4, 10^3, and 500 Å) and an RID-10A differential refractive-index detector. Calibration was achieved with commercial polystyrene standards ranging from 500 to 10^6 g/mol.

2.2. UV−Vis Spectroscopy. UV−visible spectra were recorded using a CARY 300 spectrophotometer (Bruker) equipped with a temperature controller. Molecular weight was also calculated by the following equation M_n(UV−vis) = [polymer]$_0$/ [Abs$^{305\ nm}$/ε^{RAFT}], where Abs$^{305\ nm}$, ε^{RAFT} and [polymer]$_0$ corresponding to the absorbance of RAFT agent, extinction coefficient, and polymer concentration, respectively.

2.3. NMR Spectroscopy. ^{1}H and ^{13}C NMR spectra were recorded on a Bruker ACF300 (300 MHz) or ACF500 (500 MHz) spectrometer, with D_2O or $CDCl_3$ used as solvents. Monomer conversion was determined by comparing the vinyl proton signal ($\delta \sim 5.4-6.3$, 2H/mol for methacrylamide or 3H/mol for acrylic monomers to the total CH signal ($\delta \sim 3.6-3.85$ 1H/mol for HPMA), and $-CH_2O$ ($\delta \sim 4.0-4.2$ ppm for OEG-A).

2.4. ATR-Infrared Spectroscopy. ATR FT-IR spectra were obtained using a Bruker Spectrum BX FT-IR system using diffuse reflectance sampling accessories and a resolution of 2 cm^{-1}. Each sample was analyzed using 128 scans.

2.5. Dynamic Light Scattering (DLS). Dynamic light scattering studies of the GNPs at 1 mg/mL in aqueous media were conducted using The size and ζ-potential of particles was measured by DLS which was performed using a Malvern Zetasizer Nano Series running DTS software and operating a 4 mW He−Ne laser at 633 nm. Analysis was performed at an angle of 90°. GNPs (or GNPs/polymer) solutions were prepared in distilled water with GNPs concentration of 1 mg/mL. The solution was filtered trough Millipore nylon filters (pore size 0.45 μm) to eliminate dust and large contaminants. The size measurements were carried out in quartz cuvette and the temperature was allowed to equilibrate for 5 min. The number-average hydrodynamic particle size and polydispersity index were determined by DLS (on an average of five measurements). The polydispersity index (PDI) was used to describe the width of the particle size distribution, and calculated from a cumulants analysis of the DLS measured intensity autocorrelation function and is related to the standard deviation of the hypothetical Gaussian distribution (i.e., PDI = σ^2/Z_D^2, where σ is the standard deviation and Z_D is the Z average mean size).

2.6. Transmission Electron Microscopy. The sizes and morphologies of the nanoparticles were observed using a transmission electron microscopy JEOL1400 TEM at an accelerating voltage of 100 kV. The particles were dispersed in water (1 mg/mL) and deposited onto 200 mesh, holey film, copper grid (ProSciTech) and allowed to air-dry at room temperature.

2.7. X-ray Photoelectron Spectrometer (XPS). A Kratos Axis ULTRA XPS incorporating a 165 mm hemispherical electron energy analyzer was used. The incident radiation was Monochromatic A1 X-rays (1486.6 eV) at 225 W (15 kV, 15 ma). Survey (wide) scans were taken at analyzer pass energy of 160 eV and multiplex (narrow) higher resolution scans at 20 eV. Survey scans were carried out over 1200−0 eV binding energy range with 1.0 eV steps and a dwell time of 100 ms. Narrow higher resolution scans were run with 0.2 eV steps and 250 ms dwell time. Base pressure in the analysis chamber was 1.0×10^{-9} Torr and during sample analysis 1.0×10^{-8} Torr. The data were analyzed by XPS peak 4.1.

2.8. Thermogravimetric Analysis.

Thermal Gravimetric Analysis (TGA). TGA of GNPs was performed using a Pyris 1 (Perkin-Elmer) with a rate 10 °C/min from room temperature to 650 °C. An isotherm at 100 °C maintained for 20 min to eliminate any trace of water. The weight loss was calculated from the difference between the weights at 100 °C and at 650 °C. The sample preparation was carried out according to the following procedures 100 μL of GNP solution (20 mg/mL) was placed on a TGA plate. The water was evaporated at 90 °C in the oven, and the operation was repeated yielding 3−4 mg of material. Finally, the sample was heated in the TGA to 100 °C for 20 min, and then, heating until 650 °C at a rate of 10 °C/min (see Supporting Information).

3. Syntheses. *3.1. Synthesis of Gold Nanoparticles.* GNPs was synthesized using a citrate reduction according to published procedures (for details, please see the Supporting Information).[62]

3.2. Synthesis of RAFT Agents

3.2.1. Synthesis of 3-(Benzylsulfanylthiocarbonylsulfanyl)-propionic Acid (BSPA). This RAFT agent was synthesized using an established procedure.[38]

^{1}H NMR and ^{13}C NMR confirmed the expected structure: ^{1}H NMR (300 MHz, $CDCl_3$) δ (ppm from TMS); 2.85 (2H, t, J = 6.8 Hz, $CH_2C(O)OH$), 3.62 (2H, t, SCH_2CH_2), 4.61 (2H, s, CH_2−Ph), 7.31 (5H, m, CH from (Ph). ^{13}C NMR (75 MHz, $CDCl_3$) δ (ppm from TMS): 224.1, 179.2, 136.2, 130.7, 130.1, 129.2, 42.9, 34.4, 32.3.

3.2.2. Synthesis of 4-Cyanopentanoic Acid Dithiobenzoate (CDTB). The synthesis of CDTB has been described in a previous publication and the method is detailed in the Supporting Information.[63]

^{1}H NMR and ^{13}C NMR confirmed the expected structure. ^{1}H NMR (300 MHz, $CDCl_3$), δ (ppm from TMS): 2.1 (3H, s, CH_3), 2.5 (2H, dt, $-CH_2-CH_2CO_2H$), 2.7 (2H, t, $-CH_2-COOH$), 7.2 (2H, aromatic group), 7.6 (1H, aromatic group), 7.8 ppm (2H, aromatic group). ^{13}C NMR (75 MHz, $CDCl_3$): δ (ppm from TMS): 224, 175, 145, 135, 130, 128, 126, 120, 45, 35, 32, 25.

4. RAFT Polymerizations. All of the synthesized polymers were characterized by ^{1}H NMR, gel permeation chromatography (GPC), and UV−visible spectroscopy.

4.1. RAFT Polymerization of OEG-A in the Presence of 3-(Benzylsulfanylthiocarbonylsulfanyl)propionic Acid (BSPA). An example of the polymerization of OEG-A is given for [OEG-A]$_0$/[BSPA]$_0$/[AIBN]$_0$ = 80/1/0.2. OEG-A (1.00 g, 2.2×10^{-3} mol), 3-(benzylsulfanylthiocarbonylsulfanyl)propionic acid (7.5 mg, 2.8×10^{-5} mol), AIBN (1.0 mg. 5.5×10^{-6} mol) and

acetonitrile (5 mL) were mixed. The solution was cooled in an ice bath and purged with nitrogen for 30 min before heating to 60 °C. After 8 h (conversion 70%), the solution was partially evaporated under vacuum, and the polymer was precipitated in cold diethyl ether (at 0 °C). The precipitation was repeated twice more to ensure the purity of the polymer. The product was dried in vacuo to yield a yellow powder. The synthesis of P(HPMA) is described in the Supporting Information.

4.2. Chain Extension Using MacroRAFT in the Presence of Styrene and Maleic Anhydride. A typical procedure for the chain extension of RAFT polymers prepared is described as folow: PEG macroRAFT agent (M_n = 20K, 0.1 g, 5×10^{-6} mol), styrene monomer (10 mg, 1×10^{-4} mol), maleic anhydride (10 mg, 1×10^{-4} mole) and AIBN (0.33 mg, 2×10^{-6} mole) were dissolved in dioxane (1 mL) and added to a polymerization ampule (2 mL). The ampule was sealed, the solution degassed with nitrogen for 15 min and then allowed to polymerize overnight at 60 °C. The polymerization was stopped by quenching in liquid nitrogen and the solution was partially evaporated under vacuum. The polymer was recovered by precipitation into cold diethyl ether (at 0 °C). The precipitation was repeated twice more from dichloromethane to remove any unreacted monomer. The product was dried in vacuo and characterized by SEC. A similar reaction was carried out for P(HPMA) macroRAFT, followed by a similar purification.

5. Grafting of Polymer "to" GNPs. A stirred GNP solution (10 mL of 1 mg/mL previously obtained) was placed in an ice bath under for 30 min. Polymer solution (1 mL concentration: 10 mg/L) was added to the GNP solution, followed by stirring for 30 min. Then, the GNPs were purified by centrifugation at 20 000 rpm, for 30 min at room temperature followed by resuspension in cooled water. This process was repeated 3 times. GNPs/polymer nanoparticles were stored in solution (10 mg/mL) or freeze-dried. After freeze-drying the hybrid GNP/polymer nanoparticles could be redispersed easily in water (in contrast to GNPs with no polymer coating).

6. Cross-Link Polymer Shell Using 1,2-Ethylenediamine. GNP/polymer solution (10 mL of 1 mg/mL previously obtained) was stirred, while 10 μL of 1,2-ethylenediamine was injected, along with 10 mg of EDC. The solution was stirred overnight at room temperature. A further 10 μL of 1,2-ethylenediamine was then added along with more EDC (10 mg). The cross-linking reaction was then allowed to proceed for a further 6 h, after which another addition of 1,2-ethylamine and EDC was carried out. After 24 h stirring at room temperature, the GNPs were purified by centrifugation.

7. Dissolution of Gold Core by Aqua Regia Reagent. A fresh solution of aqua regia reagent was prepared. A few aliquots (100 μL) of aqua regia reagent were added to a stirred GNPs solution (prepared above, concentration 1 mg/mL). The characteristic color of the GNPs faded rapidly. The addition was continued until total disappearance of red color. The process is very quick (less than 1 min). The solution was then dialyzed immediately against water for 24 h, with frequent changes of the water, to remove the traces of acid. The final pH of the solution was checked to ensure full removal of the acid (pH = 6.5). The solution was concentrated for further analysis by the evaporation of water at room temperature.

Results and Discussion

Two different polymers were synthesized using a trithiocarbonate (BSPA) or a dithioester RAFT agent with AIBN as the initiator for oligo(ethylene glycol) acrylate (OEG-A) or hydroxyl propylacrylamide (HPMA), respectively. At 60−70% monomer conversion, the polymerizations were stopped. After extensive purification (precipitation in diethyl ether and dialysis against water), the polymer was analyzed by UV−visible, ^{1}H NMR and SEC analyses. The presence of the RAFT end-group, vital for the directed binding to the gold surface, was confirmed i.e. a characteristic absorption at 305 nm (UV−visible); ^{1}H NMR analysis revealed signals at 2.6 ppm attributed to the $-CH_2-$ in the position adjacent to the carbonyl group (see Figure 1A for P(OEG-A) and Figure S1A (Supporting Information) for P(HPMA)). The chain-end functionality calculated by both NMR and UV−visible spectroscopy confirm that the RAFT end-group was preserved at a level greater than 90% after purification. The purified polymers were then chain extended using maleic anhydride and styrene to form a cross-linkable "b-block" (see Scheme 2). SEC analysis confirmed a shift to lower retention time (Figure S2A (Supporting Information) gives an example for P(HPMA)), in accord with increased molecular weight and a slight increase in PDI observed for the polymerization of the second block. The results of the polymer analyses are given in Table 1. The successful synthesis of the functional "b-block" was confirmed by ^{1}H NMR with the phenyl group resonances of the poly(styrene) signals observed clearly between 6.5 and 7.2 ppm. (Figure 1B for P[(OEG-A)-*b*-(Sty-*alt*-MA)]) and also by the strong absorption at 1780 cm^{-1} observed by ATR−FTIR (Figure 4A, and S3 (Supporting Infornation) for P(HPMA)) attributable to the anhydride group of the maleic anhydride monomer units. The successful purification of these polymers was investigated by ^{1}H NMR confirming the absence of any residual maleic anhydride monomer (absence of signal at 6.5 ppm).

Highly uniform spherical around 20 nm gold nanoparticles (GNP) were synthesized via the established citrate reduction method[62] (reduction of $HAuCl_4$ by boiling with sodium citrate) and characterized by both transmission electron microscopy (TEM, Figure 2A) and by dynamic light scattering (DLS, Figure S4 in the Supporting Information). The diameter of the particles obtained was around 18 nm as determined by TEM, consistent with the DLS (18 nm).

The directed assembly of the cross-linkable polymer layer was achieved using a grafting "onto" approach making use of the strong affinity of trithiocarbonate and dithioester for the gold surfaces.[32,64] Briefly, the copolymers were dissolved in THF and then added slowly to a freshly prepared solution of gold nanoparticles. After purification by centrifugation (repeated washing/centrifugation cycles), the GNPs were perfectly dispersed in water. UV−visible spectroscopy shows a slight shift in GNP plasmon absorbance from 520 to 528 nm for both samples (Figure 3A, inset shows the color evolution of the GNP solutions).

DLS analysis confirmed an increase in hydrodynamic volume of these hybrid nanoparticles in water (Figure 3B). The nanoparticle diameter distributions remained narrow and close to monodisperse (PDI determined by DLS close to 0.1). TEM images indicate the presence of stable, monodisperse nanoparticles for both copolymer systems, i.e., P[(HPMA)-*b*-(St-*alt*-MA)] and P[(OEG-A)-*b*-(St-*alt*-MA)] (see for example, Figure 2B). The populations are dominated by single nanoparticles (95%, with a diameter size around 23−26 ± 5 nm, and also, a few aggregates consisting of 2−3 particles (5%, average size 50 ± 10 nm) for P[(OEG-A)-*b*-(St-*alt*-MA)], while for P[(HPMA)-*b*-(St-*alt*-MA)], the diameter size was close to 30 nm (95% of the population, the remaining 5% consistent of a few aggregates, 50−60 nm). The presence of the copolymer surface layer was confirmed by both ATR−FTIR (Figure 4A) and XPS analysis (Figure 4B). ATR−FTIR confirmed the presence of absorptions specific to the copolymer surface composition. ATR−FTIR also confirmed that the anhydride group was not totally hydrolyzed during the aqueous coating process or subsequent purification. XPS spectra confirmed signals from carbon and oxygen originating from the P(OEG-A) and P(HPMA) blocks, respectively (Figure 4B). In addition, nitrogen was detected for P[(HPMA)-*b*-(St-*alt*-MA)] at 399 eV originating from the amide bond in the

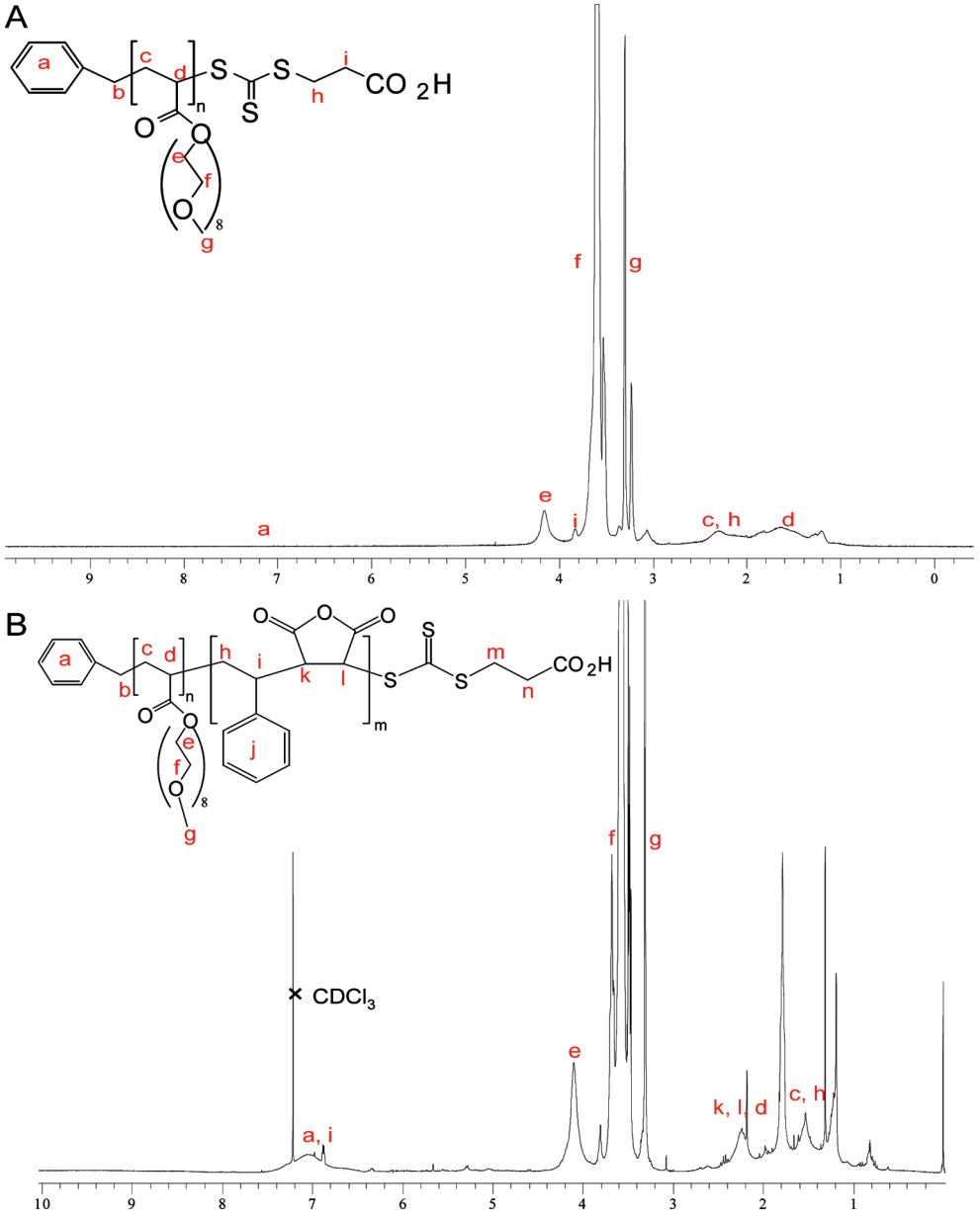

Figure 1. ^{1}H NMR spectra of A-P(OEG-A) before chain extension in D_2O (water peak was suppressed by saturation) (run #1 of Table 1); B- P[(OEG-A)-*b*-(MA-*alt*-Sty)] after chain extension in $CDCl_3$ (run #2 of Table 1).

HPMA block (data not shown). The presence of sulfur (RAFT end-group) was also detected at low concentrations. High resolution XPS confirmed the nature of S(2p) energy binding, which could be attributed to C−S−gold binding at 162.2 and 163.4 eV.[65] The hybrid nanoparticles were also characterized by TEM in the presence or absence of contrast agent. In accordance with the results obtained by DLS, the particles were well-dispersed in water. Unfortunately in the absence of contrast agent, the polymer is not visible using TEM. The addition of a negative contrast agent enhances the TEM analysis and the images indicate a clear halo around the GNPs strongly suggesting the presence of a polymer layer (Figure 2B, inset shows a magnification of one particle). Finally, the grafting density was determined by thermal gravimetric analysis (TGA) using a temperature scan from 100 to 650 °C, the weight-loss allows evaluating the packing of density according to the following equation: density = [loss weight × Na]/[(100 − loss weight)/(100 × $M_n^{Polymer}$ × $S^{Particle}$]; where weight loss is the percent weight loss corresponding to the decomposition of polymer. Na, $M_n^{Polymer}$, and $S^{particle}$ correspond to Avogadro's number, molecular weight of polymer by GPC, and specific surface of gold nanoparticles (m^2/g) calculated by the following relation: $6/(\rho \times d)$, with ρ being the volume mass of gold, i.e. 19.30 g/cm^3) and d the gold nanoparticle diameter, respectively. The grafting densities determined for both particles are relatively close 0.7 (see Table S1 in the Supporting Information). These packing densities values are close to those found previously other polymers (for instance, GNPs/P(NIPAAm), M_n = 20 kg/mol, density close to 0.9).[66]

Cross-linking of the polymer layer to stabilize the hollow polymer nanocapsules was achieved by the addition of ethylene diamine in the presence of 1-ethyl-3-(3-(dimethylamino)propyl) carbodiimide (EDC). Initial cross-linking exploits the high reactivity of the intact anhydride groups. Further cross-linking was induced using an excess of diamine and EDC to ensure the full reaction of the hydrolyzed anhydride groups, and those carboxyl groups from the anhydride-amine cross-linking events. After purification by several centrifugation/washing cycles, a rapid visual inspection confirmed that the GNPs maintained stability

Scheme 2. Illustration of Different Polymerization Steps To Yield P[(OEG-A)-*b*-(Sty-*alt*-MA)] Diblock Polymers: (a) Synthesis of P(OEG-A); (b) Chain Extension To Form P[(OEG-A)-*b*-(Sty-*alt*-MA)]

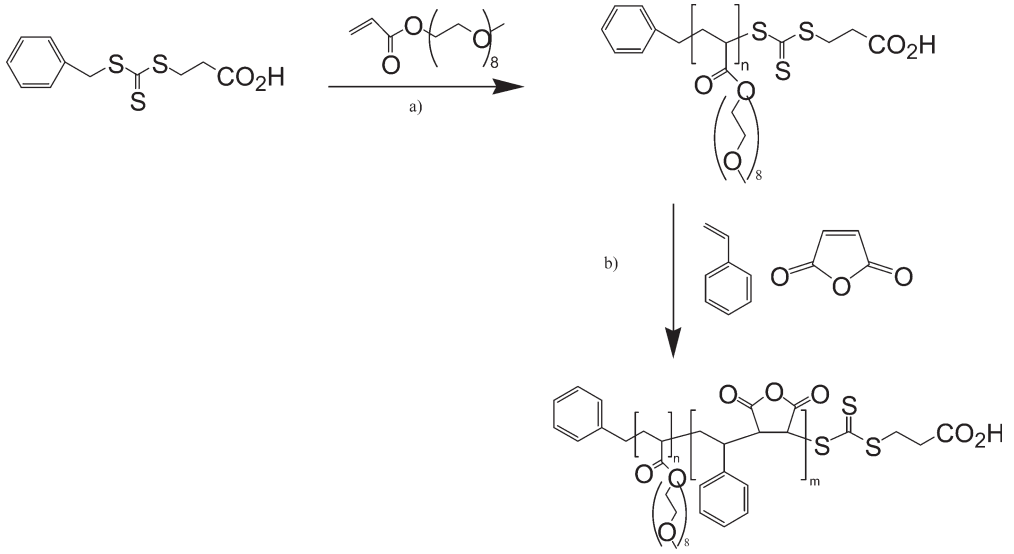

Table 1. Characteristic of Polymers Used in This Study

runs	polymers	α^M (%)[a]	M_n(theor)[b] (g/mol)	M_n (SEC)[c] [M_n (^{1}H NMR)][d] (g/mol)	PDI[c]	M_n(UV−vis)[e] (g/mol)	DP$_n$ M_1[f]	DP$_m$(Sty-*alt*-MA)[g]
1	P(OEG-A)$_n$	60	22 000	21 500 [24 200]	1.24	20 000	52	
2	P[(OEG-A)$_n$-*b*-(Sty-*alt*-MA)$_m$]	nd		26 500 [28 700]	1.35	22 000	52	22
3	P(HPMA)$_n$	70	39 500	40 500 [20 500]	1.06	22 000	140	
4	P[(HPMA)$_n$-*b*-(Sty-*alt*-MA)$_m$)	nd		46 500 [26 200]	1.12	27 000	140	29

[a] α^M (%) determined by ^{1}H NMR (see Supporting Information). [b] M_n(theor) theoretical molar mass, calculated by using the following equation: $= ([M]_0/[CTA]_0) \times \alpha^M \times MW^{Monomer} + MW^{CTA}$. [c] M_n(SEC) and PDI was determined using DMAc as mobile phase (polystyrene calibration). [d] M_n (^{1}H NMR) was calculated using the aromatic signals of RAFT agent (BSPA or CPDB, region 7.0−7.8 ppm), as reference. [e] M_n(UV−vis.) was calculated using the signal at 305 nm of RAFT end group (see equation in the experimental part). [f] DP$_n$ M_1 corresponds to average number of polymerization of OEG-A or HPMA in the copolymer calculated by NMR. [g] DP$_n$(Sty-*alt*-MA) corresponds to average number of polymerization of (Sty-*alt*-MA) in the copolymer calculated by NMR.

in water (and their characteristic red-pink color was conserved). GNPs were characterized by ATR−FTIR, XPS, DLS and UV−visible spectroscopy. ATR−FTIR confirmed the complete absence of anhydride bonds at 1788 cm^{-1} for both hybrid polymer/GNPs systems, see Figure 4A for GNPs/P[(OEG-A)-*b*-(Sty-*alt*-MA)] and Figure S3 (Supporting Information) for GNPs/P[(HPMA)-*b*-(Sty-*alt*-MA)]. However, the absence of the anhydride bonds can be attributed to either hydrolysis products of the anhydride or a successful cross-linking reaction. In the case of P[(OEG-A-*b*-(St-*alt*-MA))], the formation of a shoulder on the absorption at 1690 cm^{-1} (partially overlapped with the ester bond absorption at 1730 cm^{-1} from the P(OEG) block) was indicative of the successful formation of amide bonds. However, it is important to note that the absorption of carboxylic acid is close to this region (1710−1715 cm^{-1}). XPS analyses were invoked to investigate the presence and nature of nitrogen on the surface (i.e., amine or amide). The presence of nitrogen groups was confirmed for the shell cross-linked polymer/GNP hybrids. Using high resolution XPS, two different nitrogen signals were identified in the region of N (1s): 399.9 eV and at 401.5 eV that were attributed to the amide bond and the protonated amine ($-NH_3^+$ or $-NH_2^+$) (Figure S5 (Supporting Information)).[65] In addition, the nature of sulfur was also investigated by XPS using a high resolution XPS in the region at 160−166 eV. It is interesting to note the characteristic S(2p) of RAFT end group disappeared, while a covalent −S−Au signal at 163.2−164.4 eV appeared. This reveals that the RAFT end group was degraded during the cross-linking process via aminolysis process to form a thiol.[67] Finally, the nature of the anhydride group was also investigated by XPS. The characteristic peak at 289.4 eV attributed to the carbonyl group of anhydride[68] disappeared after reaction with amine and a new signal appears at 287.2 eV attributed to amide bond (C(1s) of *C*O−NH). ATR−FTIR analyses of the GNPs coated with P(HPMA) copolymers, did not indicate any free carboxylic acid groups (shown by the absence of any absorption at 1715 cm^{-1}) and anhydride groups. A similar XPS on P[(HPMA)-*b*-(St-*alt*-MA)] cross-linked hybrid nanoparticles was compromised by the presence of a large nitrogen signal originating from the P(HPMA) block. DLS analyses indicate a slight shift to higher hydrodynamic volumes after cross-linking following a partial destabilization of GNPs during the cross-linking phase. This observation is consistent with UV−visible spectroscopy which shows a slight shift in a resonance binding 535 nm. Successful polymer coating of the nanoparticles polymers was also confirmed by TEM (using a negative contrast agent) showing clear halos around the GNPs indicative of an enveloping polymer layer.

A control experiment (inspired by Matyjaszewski's work[69]) was performed for both polymers to confirm the presence of a

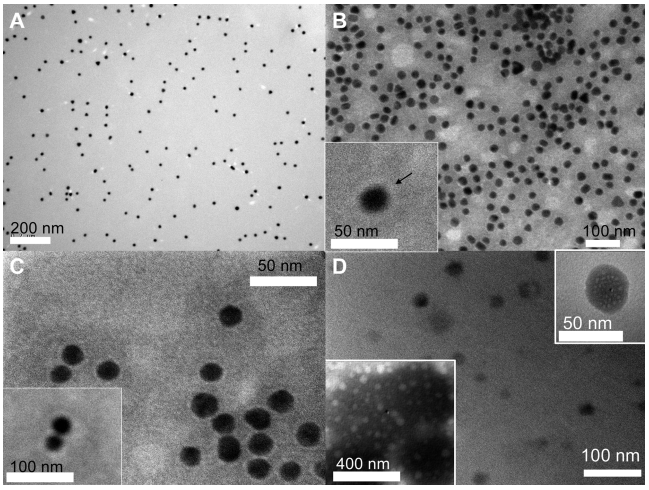

Figure 2. TEM analysis: (A) naked GNPs (20 nm) synthesized for this study; (B) GNPs coated P[(OEG-A)-*b*-(Sty-*alt*-MA)), run no. 2 of Table 1; (C) GNPs/P[(OEG-A)-*b*-(Sty-*alt*-MA)) after cross-linking; (D) P[(HPMA)-*b*-(Sty-*alt*-MA)) (run no. 4 of Table 1) hollow nanocapsule (full picture-no contrast agent). The picture inset top-right corner is a magnified images of these particles and the inset bottom-left is a picture of the same solution using a negative contrast agent.

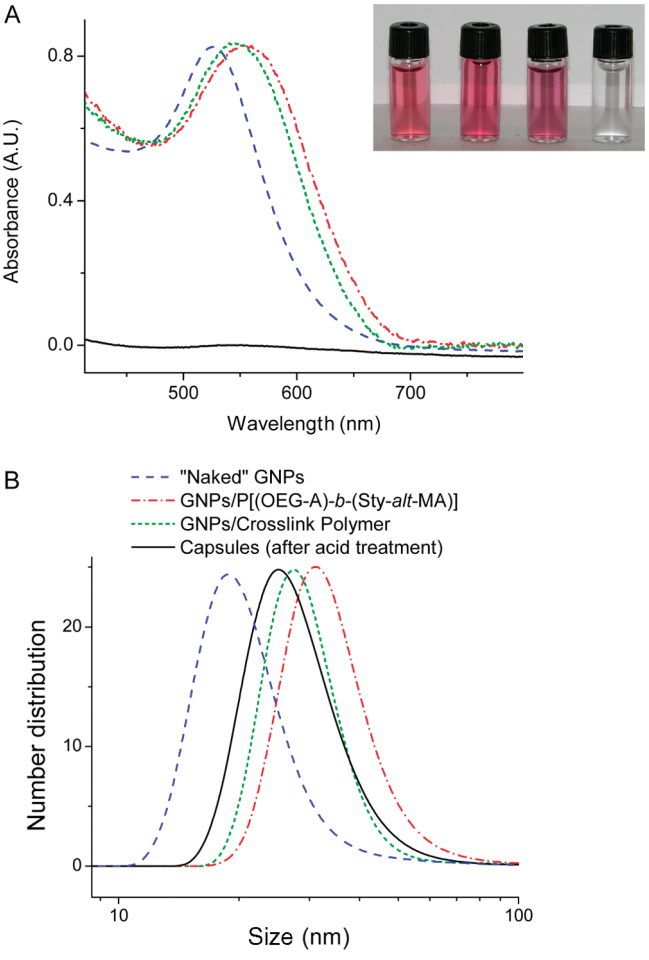

Figure 3. Characteristics of GNPs/P[(OEG-A)-*b*-(Sty-*alt*-MA)), run #1 of Table 1, during hollow capsule formation. (A) UV−visible spectra of GNPs, concentration: 5 mg/mL (inset: pictures of GNP solutions and nanocaspules). (B) Dynamic light scattering analysis of same materials (concentration 5 mg/mL).

cross-linked shell around the GNPs, by testing the stability of our GNP solutions at high temperature. In the absence of a

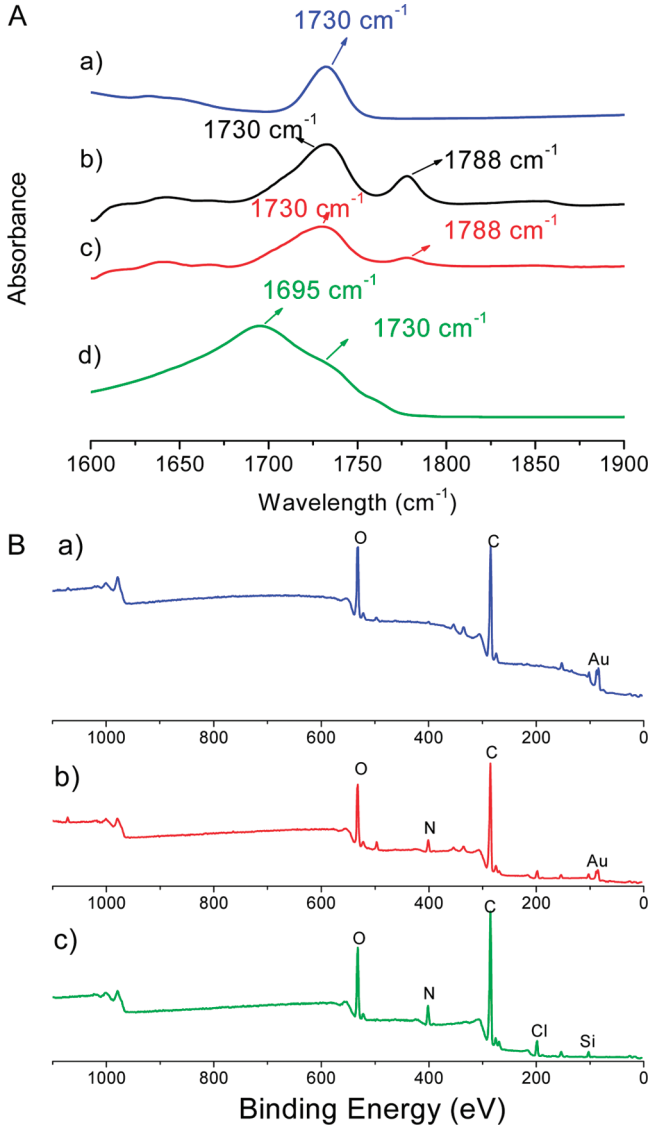

Figure 4. Surface analysis of GNPs/P[(OEG-A)-*b*-(Sty-*alt*-MA)) (run #2 of Table 1) using ATR−FTIR and XPS. (A) ATR−FTIR analysis: (a) P(OEG-A) before chain extension run #1 of Table 1); (b) P[(OEG-A)-*b*-(MA-*alt*-Sty)], run no. 2 of Table 1; (c) after cross-linking using a diamine (first addition of 10 μL of diamine) on GNP surfaces; (d) after addition of excess diamine on GNPs (second addition of diamine). (B) XPS analysis: (a) GNPs/P[(OEG-A)-*b*-(Sty-*alt*-MA)] before cross-linking, run no. 1 of Table 1; (b) purified GNPs/P[(OEG-A)-*b*-(Sty-*alt*-MA)] after cross-linking; (c) capsules after acid treatment on silica plate.

cross-linked shell, our GNPs precipitate as the thiol−gold bond cleaves above 60 °C, as reported in a previous article.[69] In the presence of a cross-linked shell, the GNPs remain perfectly dispersed overnight at 80 °C as confirmed by visual inspection and by DLS analysis (diameter size around 40 nm, see Figure S11 in the Supporting Information). The plasmon resonance of these cross-linked polymer GNPs before and after treatment stays close to 525 nm, while in the case of non cross-linked polymer present a higher plasmon resonance. (around 600 nm, Figure S12 in the Supporting Information) characteristic of destabilized nanoparticles This outcome supports the presence of a cross-linked polymer shell that physically encompasses the GNPs.

The gold cores were removed using an aqua regia reagent. Aqua regia was added dropwise to a stirred solution of the shell cross-linked nanoparticles until the characteristic pink-red color of the solution disappeared (Figure 3A, inset) (reaction time around 1 min). The solution was then rapidly dialyzed using

a membrane cutoff 8 000 Da against a large volume of Ultra pure water to quickly and efficiently remove the aqua regia reagent. UV−visible analysis confirmed the absence of the characteristic resonance band of gold (Figure 3A and Figure S6)Supporting Information)); however, DLS analyses confirmed the presence of nanoparticles with slightly smaller sizes than the original hybrid polymer GNPs. This slight decrease can be attributed to solvophobic contraction of the phenyl containing core. In addition, ζ-potential studies show the absence of charged particles (∼0 mV). A comparison of XPS spectra taken before and after reaction with the aqua regia reagent, confirmed the loss of gold and the retention of the polymeric component (the characteristics peaks (C and O) of polymers were unaffected by the acid treatment, Figure 4B). The presence of chlorine (Cl ($2p^3$)) at 197.9 eV was also observed and can be attributed to complexation with the free amine ($-NH_3^+/Cl^-$).[65] A further control experiment was conducted to investigate the effect of the strong acid conditions on the overall integrity of the polymeric structures. P(HPMA) or P(OEG-A)) were exposed to the aqua regia for 1 h (60 times longer than the conditions used for nanoparticle modification), followed by dialysis against water, and then freeze-drying. ^{1}H NMR and GPC analyses show that the polymers were unaffected by this treatment (data in Supporting Information, Figures S7 and S8). However, UV−visible spectroscopy indicated the loss of RAFT agent (λ = 305 nm) after the acid treatment, suggesting that the RAFT end-group could be lost during either the cross-linking process (aminolysis) or via exposure to the aqua regia reagent (Figure S9); we are conducting further studies on the precise mechanism of this reaction in aqua regia.

The formation of hollow polymer nanoparticles, P[(HPMA)-*b*-(St-*alt*-MA)] and P[(OEG-A)-*b*-(St-*alt*-MA)] was also strongly supported by TEM analyses. TEM images, acquired without contrast agent, clearly indicate the absence of gold cores (in accord with the UV−visible spectroscopy data). The hollow polymer capsules are clearly observed (Figure 2D and Figure S10 in the Supporting Information). Analysis of the TEM images show that the capsule diameter sizes are slightly smaller than those measured by DLS, which can be attributed to the anhydrous conditions under which the TEM images are acquired. The average diameter size is 30 ± 5 nm (proportion 90%), with the presence of large capsules around 40−50 nm (proportion 10%) in the case of cross-linked P(OEG-A-*b*-(Sty-*alt*-MA). Cross-linked P(HPMA-*b*-(Sty-*alt*-MA)] yielded slightly larger diameter sizes (around 45 ± 5 nm) than P(OEG-A-*b*-(Sty-*alt*-MA). To improve the resolution, a negative contrast agent was added, confirming polymer nanoparticles with similar sizes to those found earlier (Figure 2D inset and Figure S11, inset). The images are in good agreement with those obtained by other researchers for hollow polymer nanoparticles of approximately this size, synthesized via different templated processes.

Conclusion

This paper describes a new route to the synthesis of hollow nanoparticles using gold nanoparticles as sacrificial templates for polymers obtained by RAFT polymerization. Polymers were cross-linked onto the gold templates, followed by gold removal using aqua regia at room temperature. XPS, FT-IR, UV−vis, and DLS confirmed both the cross-linking of the polymer nanoshell, the complete removal of the gold nanoparticle core and the stability of the hollow polymer nanocapsules. Further investigations are in progress to determine the encapsulation ability of these particles.[20]

Acknowledgment. The authors thank the Australian Research Council for funding and TPD acknowledges the award of a Federation Fellowship.

Supporting Information Available: Text giving experimental information, figures of ^{1}H NMR spectra of P(HPMA) before and after chain extension, SEC traces, TEM pictures of capsules, and XPS, ATR−FTIR, DLS, TGA, and UV−visible results for GNPs/P(HPMA), and a table of grafting density. This material is available free of charge via the Internet at http://pubs.acs.org.

References and Notes

(1) Meier, W. *Chem. Soc. Rev*. **2000**, *29*, 295–303.
(2) Johnston, A. P. R.; Cortez, C.; Angelatos, A. S.; Caruso, F. *Curr. Opin. Colloid Interface Sci*. **2006**, *11*, 203.
(3) Chong, S.-F.; Sexton, A.; De Rose, R.; Kent, S. J.; Zelikin, A. N.; Caruso, F. *Biomaterials* **2009**, *30*, 5178.
(4) Yu, A. M.; Gentle, I.; Lu, G. Q.; Caruso, F. *Chem. Commun*. **2006**, 2150.
(5) Sukhorukov, G. B.; Rogach, A. L.; Zebli, B.; Liedl, T.; Skirtach, A. G.; Köhler, K.; Antipov, A. A.; Gaponik, N.; Susha, A. S.; Winterhalter, M.; Parak, W. J. *Small* **2004**, *1*, 194–200.
(6) Musyanovych, A.; Landfester, K. *Prog. Colloid Polym. Sci*. **2008**, *134*, 120–127.
(7) Paiphansiri, U.; Tangboriboonrat, P.; Landfester, K. *Macromol. Biosci*. **2006**, *6*, 33–40.
(8) O'Reilly, R. K.; Joralemon, M. J.; Hawker, C. J.; Wooley, K. L. *J. Polym. Sci., Part A: Polym. Chem*. **2006**, *44*, 5203–5217.
(9) McCormick, C. L.; Sumerlin, B. S.; Lokitz, B. S.; Stempka, J. E. *Soft Matter* **2008**, *4*, 1760–1773.
(10) Rimmer, S.; Ramli, A. N. M.; Lefèvre, S. *Polymer* **1996**, *37*, 4135–4139.
(11) Rimmer, S.; Carter, S.; Rutkaite, R.; W.Haycock, J.; Swanson, L. *Soft Matter* **2007**, *3*, 971–973.
(12) Wang, Y.; Angelatos, A. S.; Caruso, F. *Chem. Mater*. **2008**, *20*, 848.
(13) Yap, H. P.; Hao, X.; Tjipto, E.; Gudipati, C.; Quinn, J. F.; Davis, T. P.; Barner-Kowollik, C.; Stenzel, M. H.; Caruso, F. *Langmuir* **2008**, *24*, 8981.
(14) Read, E. S.; Armes, S. P. *Chem. Commun*. **2007**, *29*, 3021–3035.
(15) Connal, L. A.; Kinnane, C. R.; Zelikin, A. N.; Caruso, F. *Chem. Mater*. **2009**, *21*, 576–578.
(16) O'Reilly, R. K.; Joralemon, M. J.; Hawker, C. J.; Wooley, K. L. *New J. Chem*. **2007**, *31*, 718–724.
(17) Zhang, Q.; Remsen, E. E.; Wooley, K. L. *J. Am. Chem. Soc*. **2000**, *122*, 3642–3651.
(18) Joralemon, M. J.; Murthy, K. S.; Remsen, E. E.; Becker, M. L.; Wooley, K. L. *Biomacromolecules* **2004**, *5*, 903–913.
(19) Murthy, K. S.; Ma, Q.; Remsen, E. E.; Kowalewski, T.; Wooley, K. L. *J. Mater. Chem*. **2003**, *13*, 2785–2795.
(20) Huang, H.; Remsen, E. E.; Kowalewski, T.; Wooley, K. L. *J. Am. Chem. Soc*. **1999**, *121*, 3805–3806.
(21) Fang, H.; Zhang, K.; Shen, G.; Wooley, K. L.; Taylor, J.-S. A. *Mol. Pharmaceutics* **2009**, *6*, 615–626.
(22) Liu, X.; Basu, A. *J. Am. Chem. Soc*. **2009**, *131*, 5718–5719.
(23) Chen, Y.; Cho, J.; Young, A.; Taton, T. A. *Langmuir* **2007**, *23*, 7491–7497.
(24) Duan, H.; Kuang, M.; Zhang, G.; Wang, D.; Kurth, D. G.; Moehwald, H. *Langmuir* **2005**, *21*, 11495–11499.
(25) Chandrawati, R.; Städler, B.; Postma, A.; Connal, L. A.; Chong, S.-F.; Zelikin, A. N.; Caruso, F. *Biomaterials* **2009**, *30*, 5988.
(26) Zelikin, A. N.; Quinn, J. F.; Caruso, F. *Biomacromolecules* **2006**, *7*, 27.
(27) Schneider, G.; Decher, G. *Nano Lett*. **2004**, *4*, 1833–1839.
(28) Schneider, G. F.; Decher, G. *Nano Lett*. **2008**, *8*, 3598–3604.
(29) Boyer, C.; Bulmus, V.; Davis Thomas, P.; Ladmiral, V.; Liu, J.; Perrier, S. *Chem. Rev*. **2009**, *109*, 5402–5436.
(30) Boyer, C.; Whittaker, M.; Luzon, M.; Davis, T. P. *Macromolecules* **2009**, *42*, 6917–6926.
(31) Roth, P. J.; Theato, P. *Chem. Mater*. **2008**, *20*, 1614–1621.
(32) Hotchkiss, J. W.; Lowe, A. B.; Boyes, S. G. *Chem. Mater*. **2007**, *19*, 6–13.
(33) Duwez, A.-S.; Guillet, P.; Colard, C.; Gohy, J.-F.; Fustin, C.-A. *Macromolecules* **2006**, *39*, 2729–2731.
(34) Lowe, A. B.; Sumerlin, B. S.; Donovan, M. S.; McCormick, C. L. *J. Am. Chem. Soc*. **2002**, *124*, 11562–11563.
(35) Sumerlin, B. S.; Lowe, A. B.; Stroud, P. A.; Zhang, P.; Urban, M. W.; McCormick, C. L. *Langmuir* **2003**, *19*, 5559–5562.
(36) Scales, C. W.; Convertine, A. J.; McCormick, C. L. *Biomacromolecules* **2006**, *7*, 1389–1392.

(37) York, A. W.; Scales, C. W.; Huang, F.; McCormick, C. L. *Biomacromolecules* **2007**, *8*, 2337–2341.
(38) Boyer, C.; Bulmus, V.; Davis, T. P. *Macromol. Rapid Commun.* **2009**, *30*, 493–497.
(39) Zareie, H. M.; Boyer, C.; Bulmus, V.; Nateghi, E.; Davis, T. P. *ACS Nano* **2008**, *2*, 757–765.
(40) Boyer, C.; Liu, J.; Bulmus, V.; Davis Thomas, P. *Aust. J. Chem.* **2009**, *62*, 830–847.
(41) Jia, Z.; Liu, J.; Boyer, C.; Davis Thomas, P.; Bulmus, V. *Biomacromolecules* **2009**, DOI:10.1021/bm900817a.
(42) Kakwere, H.; Perrier, S. *J. Am. Chem. Soc.* **2009**, *131*, 1889–1895.
(43) Suchao-in, N.; Chirachanchai, S.; Perrier, S. *Polymer* **2009**, *50*, 4151–4158.
(44) Sun, G.; Fang, H.; Cheng, C.; Lu, P.; Zhang, K.; Walker, A. V.; Taylor, J.-S. A.; Wooley, K. L. *ACS Nano* **2009**, *3*, 673–681.
(45) Inoue, S.; Kakikawa, H.; Nakadan, N.; Imabayashi, S.-i.; Watanabe, M. *Langmuir* **2009**, *25*, 2837–2841.
(46) Raula, J.; Shan, J.; Nuopponen, M.; Niskanen, A.; Jiang, H.; Kauppinen, E. I.; Tenhu, H. *Langmuir* **2003**, *19*, 3499–3504.
(47) Kim, D. J.; Kang, S. M.; Kong, B.; Kim, W.-J.; Paik, H.-j.; Choi, H.; Choi, I. S. *Macromol. Chem. Phys.* **2005**, *206*, 1941–1946.
(48) Shan, J.; Zhao, Y.; Granqvist, N.; Tenhu, H. *Macromolecules* **2009**, *42*, 2696–2701.
(49) Aqil, A.; Qiu, H.; Greisch, J.-F.; Jerome, R.; De Pauw, E.; Jerome, C. *Polymer* **2008**, *49*, 1145–1153.
(50) Zhang, T.; Zheng, Z.; Ding, X.; Peng, Y. *Macromol. Rapid Commun.* **2008**, *29*, 1716–1720.
(51) Boyer, C.; Bulmus, V.; Priyanto, P.; Teoh, W. Y.; Amal, R.; Davis, T. P. *J. Mater. Chem.* **2009**, *19*, 111–123.
(52) Boyer, C.; Priyanto, P.; Davis, T. P.; Pissuwan, D.; Bulmus, V.; Kavallaris, M.; Teoh, W. Y.; Amal, R.; Carroll, M.; Woodward, R.; Pierree, T. S. *J. Mater. Chem.* **2010**, *20*, 255–265.
(53) Huang, Y.; Liu, Q.; Zhou, X.; Perrier, S.; Zhao, Y. *Macromolecules* **2009**, *42*, 5509–5517.
(54) Roth, P. J.; Jochum, F. D.; Zentel, R.; Theato, P. *Biomacromolecules* **2009**, DOI:10.1021/bm901249n.
(55) Gittins, D. I.; Caruso, F. *Adv. Mater.* **2000**, *12*, 1947–1949.
(56) (a) Boyer, C.; Liu, J.; Wong, L.; Tippett, M.; Bulmus, V.; Davis, T. P. *J. Polym. Sci., Part A: Polym. Chem.* **2008**, *46*, 7207–7224. (b) Roth, P. J.; Haase, M.; Basch, M.; Theato, P.; Zentel, R. *Macromolecules* ASAP, DOI: 10.1021/ma902391b.
(57) Tao, L.; Liu, J.; Xu, J.; Davis, T. P. *Chem. Commun.* **2009**, 6560–6562.
(58) (a) Xu, J.; Boyer, C.; Bulmus, V.; Davis, T. P. *J. Polym. Sci., Part A: Polym. Chem.* **2009**, *47*, 4302–4313. (b) York, A. W.; Scales, C. W.; Huang, F.; McCormick, C. *Biomacromolecules* ASAP, DOI: 10.1021/bm901249. (c) York, A. W.; Zhang, Y.; Holley, A. C.; Guo, Y.; Huang, F.; McCormick, C. *Biomacromolecules* **2009**, *10*, 936–943.
(59) Hao, X.; Stenzel, M. H.; Barner-Kowollik, C.; Davis, T. P.; Evans, E. *Polymer* **2004**, *45*, 7401–7415.
(60) Harrisson, S.; Wooley, K. L. *Chem. Commun.* **2005**, 3259–3261.
(61) Pissuwan, D.; Boyer, C.; Gunasekaran, K.; Davis, T. P.; Bulmus, V. *Biomacromolecules*, in press; DOI:10.1021bm901129x.
(62) Frens, G. *Nat. Phys. Sci.* **1973**, *241*, 20–22.
(63) Scales, C. W.; Vasilieva, Y. A.; Convertine, A. J.; Lowe, A. B.; McCormick, C. L. *Biomacromolecules* **2005**, *6*, 1849.
(64) Duwez, A.-S.; Guillet, P.; Colard, C.; Gohy, J.-F.; Fustin, C.-A. *Macromolecules* **2006**, *39*, 2729–2731.
(65) Beamson, G.; Briggs, D. *High Resolution XPS of Organic Polymers*; John Wiley and Sons: Chichester, U.K., 1992.
(66) Boyer, C.; Whittaker, M.; Chuah, K.; Liu, J.; Davis, T. P. *Langmuir*, ASAP, DOI: 10.1021/la902746v.
(67) Boyer, C.; Granville, A.; Davis, T. P.; Bulmus, V. *J. Polym. Sci., Part A: Polym. Chem.* **2009**, *47*, 3773–3794.
(68) Tang, W.; Chen, Q.; Zhang, Y.; Ge, Y. *Plasma Sci. Technol.* **2008**, *10*, 176–179.
(69) Dong, H.; Zhu, M.; Yoon, J. A.; Gao, H.; Jin, R.; Matyjaszewski, K. *J. Am. Chem. Soc.* **2008**, *130*, 12852–12853.